TimeFilter: Patch-Specific Spatial-Temporal Graph Filtration for Time Series Forecasting

Yifan Hu 1* Guibin Zhang 2* Peiyuan Liu 1* Disen Lan 3 Naiqi Li 1 Dawei Cheng 4 Tao Dai 5 Shu-Tao Xia 1 Shirui Pan 6

Abstract

Time series forecasting methods generally fall into two main categories: Channel Independent (CI) and Channel Dependent (CD) strategies. While CI overlooks important covariate relationships, CD captures all dependencies without distinction, introducing noise and reducing generalization. Recent advances in Channel Clustering (CC) aim to refine dependency modeling by grouping channels with similar characteristics and applying tailored modeling techniques. However, coarse-grained clustering struggles to capture complex, time-varying interactions effectively. To address these challenges, we propose TimeFilter, a GNN-based framework for adaptive and fine-grained dependency modeling. After constructing the graph from the input sequence, TimeFilter refines the learned spatial-temporal dependencies by filtering out irrelevant correlations while preserving the most critical ones in a patch-specific manner. Extensive experiments on 13 real-world datasets from diverse application domains demonstrate the state-of-the-art performance of TimeFilter. The code is available at https://github.com/ TROUBADOUR000/TimeFilter.

1. Introduction

Multivariate time series forecasting is a challenging task due to the need to capture both temporal dynamics and inter-channel dependencies. This problem arises in a wide range of real-world applications, including weather forecast-

Proceedings of the 42nd International Conference on Machine Learning, Vancouver, Canada. PMLR 267, 2025. Copyright 2025 by the author(s).

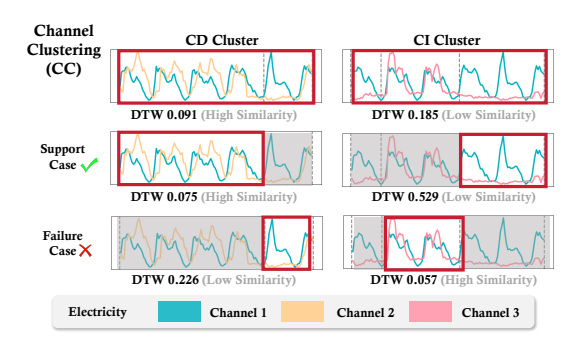


Figure 1. Analysis of three channels from the Electricity dataset shows the pros and cons of CI, CD, and CC strategies in different cases. Dynamic Time Warping (DTW) is a metric for measuring the similarity between two sequences, with lower values indicating higher similarity. The CI strategy ignores the highly correlated covariate information in the Supporting Case (left). The CD strategy fuses all information, including the irrelevant dependencies in the Supporting Case (right). The CC strategy addresses these issues by using global correlation to form CD and CI clusters. However, it cannot model the dynamic interactions of channels at different time steps at a fine-grained level. For example, in the Failure Case, it still faces the same dilemma as CD and CI strategies.

ing (Volkovs et al., 2024), traffic flow analysis (Shu et al., 2021), health monitoring (Morid et al., 2023), and financial investment (Zhu et al., 2024a;b). The literature on deep learning approaches for this task can be broadly categorized into channel-independent (CI) methods and channel-dependent (CD) methods (Han et al., 2024b).

CI methods rely on the individual historical values of each channel for prediction (Nie et al., 2023; Dai et al., 2024; Zeng et al., 2023), while CD methods go a step further by modeling the dependencies between different channels (Yu et al., 2024; Huang et al., 2023; Zhang & Yan, 2023). However, it is important to recognize that data from different domains often exhibit significant variations in underlying distributions and characteristics. For instance, in climaterelated data, there are typically natural physical dependencies among variables (Karevan & Suykens, 2020), whereas in electricity consumption data, the usage patterns of individual users can vary drastically, with little to no interdependence. This stark contrast suggests that the assumption

^{*}Equal contribution ¹Tsinghua Shenzhen International Graduate School, Tsinghua University ²National University of Singapore ³Fudan University ⁴Tongji University ⁵Shenzhen University ⁶Griffith University. Correspondence to: Tao Dai <daitao.edu@gmail.com>, Shirui Pan <s.pan@griffith.edu.au>.

of channel independence in CI methods, as well as the indiscriminate modeling of inter-channel dependencies in CD methods, both have inherent limitations.

To address this challenge, recent works have introduced the concept of Channel Clustering (CC), where channels with similar patterns are grouped into clusters based on data-dependent criteria. For instance, CCM (Chen et al., 2024) dynamically clusters channels with inherent similarities, applying CD modeling within each cluster and CI modeling across different clusters. However, CCM only considers relationships within the same cluster. DUET (Qiu et al., 2024b), on the other hand, extends this idea by introducing clustering in the temporal dimension as well. By dynamically assigning different modeling strategies for inter-cluster and intra-cluster relationships, these approaches enhance forecasting capabilities by effectively capturing both intra-cluster and inter-cluster dependencies.

Despite their success, it is notable that existing CC methods typically rely on a coarse-grained approach, where similarity across channels is calculated using data from all time points for clustering. As illustrated in Figure 1, this coarse-grained clustering fails to flexibly select appropriate dependency modeling strategies for specific time periods. The complex dependencies between channels evolve over time, and channels that are closely related within a cluster may become completely independent at certain time intervals. In such cases, applying a CD method could lead to overfitting (Zhao & Shen, 2024). Conversely, channels that are unrelated in the overall cluster may become highly correlated at exact times, and using a CI method would risk losing valuable inter-variable information. This limitation underscores the need for more dynamic and adaptive approaches that can capture time-varying dependencies.

Motivated by the observations above, we transition from previous coarse-grained, channel-wise clustering approaches to a finer-grained, patch-wise partitioning strategy, where each channel is divided into non-overlapping segments. With this partitioning, as shown in Figure 2(b), there are three key types of relationships: **1** temporal dependencies between different patches within the same channel, **2** inter-channel (spatial) dependencies at the same time step, and **3** spatial-temporal dependencies between different channels and time periods. These relationships are often intricately intertwined in real-world time series data. To more robustly model these complex dependencies, we further design a filtering method for each dependency region, effectively removing irrelevant noisy relationships and ensuring that only the most significant connections are considered.

Technically, we propose TimeFilter, a novel framework crafted to capture intricate spatiotemporal dependencies across both temporal and spatial dimensions, while dynamically filtering out extraneous information. Specifically,

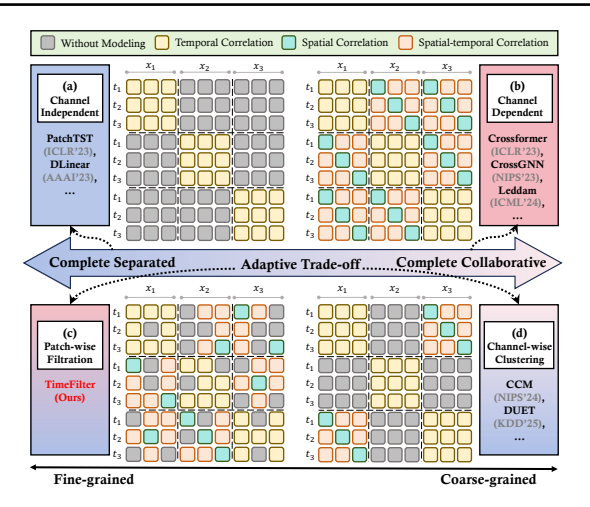


Figure 2. The dependency map of 4 different strategies. t_i is the time step and x_i is one channel. (a) CI strategy preserves only the temporal dependencies. (b) CD strategy fuses all dependencies. (c) Patch-wise Filtration finely selects dependencies for each patch. (d) Channel-wise Clustering coarsely models channel dependencies.

TimeFilter begins with **Spatial-Temporal Construction Module**, which segments the input time series into non-overlapping patches and constructs a spatial-temporal graph. After that, **Patch-Specific Filtration Module** applies a Mixture of Experts (MoE)-style dynamic router to filter out redundant dependencies, honing in on the most critical spatiotemporal relationships. Finally, **Adaptive Graph Learning Module** leverages the graph structure to aggregate relevant information and produce accurate forecasting results. Extensive experiments on several datasets show that Time-Filter achieves consistent state-of-the-art performance in both long- and short-term forecasting. Our contributions can be summarized as follows:

- Novel Paradigm. We for the first time advocate for a fine-grained segmentation of dependencies, capturing spatial-temporal relationships at the patch level while adaptively filtering out irrelevant information.
- 2 Technical Contribution. We propose TimeFilter, a novel dependency modeling strategy that employs patch-specific filtration to learn better omni-series representations for time series forecasting.
- **6** Holistic Evaluation. Comprehensive experiments demonstrate that TimeFilter achieves state-of-the-art performance in both long- and short-term forecasting, with error reductions of 4.48% and 5.34%, respectively.

2. Related Work

2.1. Multivariate Time Series Forecasting

Multivariate time series forecasting (MTSF) has widespread applications in various domains. In recent years, deep learn-

ing models have shown great promise in MTSF. RNN-based methods (Lin et al., 2023), leveraging the Markov assumption, model the sequential nature by considering current and previous time steps. CNN-based methods (Dai et al., 2024; Wu et al., 2023) apply convolution operations along the time dimension to capture local temporal patterns. However, they struggle with long-term dependencies due to vanishing gradients and limited receptive fields, respectively. Transformer-based methods (Liu et al., 2024b;a) use attention mechanisms to model long-term temporal dependencies, yielding strong performance. However, they tend to overlook the sequential nature of time series, which is crucial for maintaining temporal consistency. MLP-based methods (Hu et al., 2024; Yu et al., 2024), with their dense weights, capture interactions between different time steps in a simple but effective way. Their straightforward architecture makes them a popular choice for time series forecasting tasks. Additionally, GNN-based methods (Wu et al., 2020; Huang et al., 2023) are applied to capture the relationships between different variables in a graph structure.

2.2. Dependency Modeling

Regarding modeling dependencies in MTSF, some models adopt a Channel Independence (CI) strategy (Nie et al., 2023; Zeng et al., 2023; Lin et al., 2024), as in Figure 2(a), preserving only the temporal dependencies. These models use only the historical information of each individual sequence, ignoring the interactions between variables. Although the CI approach is robust, it wastes the potentially relevant relationships from inter-channel information. In contrast, the Channel Dependency (CD) strategy (Liu et al., 2024b; Zhang & Yan, 2023; Yu et al., 2024), as in Figure 2(b), models the full spectrum of information, providing information gains but also including redundant dependencies, thus reducing robustness. Therefore, designing an adaptive dependency modeling strategy remains a significant challenge. Recent research (Chen et al., 2024; Qiu et al., 2024b) employs a Channel Clustering (CC) strategy to dynamically select modeling strategies based on channel similarity, as in Figure 2(d). For instance, variables x_1 and x_3 are chosen to form a CD cluster, where inter-channel relationships are modeled, while variable x_2 is assigned to a CI cluster, relying only on its own historical values. However, this coarse-grained approach fails to capture the dynamically evolving interactions. Therefore, as in Figure 2(c), we design a robust and fine-grained filtering mechanism to customize the dependencies needed for each time segment.

3. Preliminaries

3.1. Problem Definition

In the multivariate time series forecasting task, let $\mathbf{X} = \{\mathbf{x_1}, \mathbf{x_2}, ..., \mathbf{x_C}\} \in \mathbb{R}^{C \times L}$ be the input time series,

where C denotes the number of channels and L denotes the look-back horizon. $\mathbf{x_i} \in \mathbb{R}^L$ represents one of the channels. The objective is to construct a model that predicts the future sequences $\mathbf{Y} = \{\hat{\mathbf{y}_1}, \hat{\mathbf{y}_2}, ..., \hat{\mathbf{y}_C}\} \in \mathbb{R}^{C \times T}$, where T denotes the forecasting horizon.

3.2. Dependency Matrix

The dependency matrix $\mathbf{M} \in \mathbb{R}^{n \times n}$ describes the dependencies within channels at different time patches as the adjacency matrix of a spatial-temporal graph $\mathcal{G} = \{\mathcal{V}, \mathcal{E}\}$ with \mathcal{V} as the node set and \mathcal{E} as the edge set, where $n = C \times N$ and N denotes the number of patches in the look-back sequence. \mathbf{M} is utilized to depict the inter-node relationship, where $\mathbf{M}[i,j]$ indicates the weight of edge $e_{ij} \in \mathcal{E}$.

Moreover, we decompose $\mathcal G$ into patch-specific ego graphs $\{\mathcal G_i\}_1^n$. Each central node of the graph $\mathcal G_i$ represents the specific patch of input sequence. Then each ego graph $\mathcal G_i$ is divided into three subgraphs: spatial subgraph $\mathcal G_i^S$, temporal subgraph $\mathcal G_i^T$, and spatial-temporal subgraph $\mathcal G_i^{ST}$. Each subgraph describes a different type of dependency of a specific patch. The adjacency matrix of each subgraph can be obtained by applying masks to $\mathbf M$.

4. Method

The core of TimeFilter, as illustrated in Figure 3, is to capture fine-grained spatial-temporal dependencies through three key components: (i) Spatial-Temporal Construction Module segments the input sequence into non-overlapping patches and constructs the spatial-temporal graph; (ii) Patch-Specific Filtration Module filters out irrelevant information through the Mixture of Experts (MoE) with Dynamic Routing mechanism to obtain the spatial-temporal dependencies for the current sequence; (iii) Adaptive Graph Learning Module leverages the graph structure to aggregate pertinent information and derives the forecasting results. The details of each essential module are explained in the following subsections.

4.1. Spatial-Temporal Construction (STC) Module

In this stage, we construct the spatial-temporal graph using the input look-back sequence. First, each channel of the input sequence $\mathbf{X} \in \mathbb{R}^{C \times L}$ is divided into non-overlapping patches $\mathbf{X}_p' \in \mathbb{R}^{C \times N \times P}$, where each patch has a length of P and the number of patches $N = \lceil \frac{L}{P} \rceil$. Then each patch is mapped to an embedded patch token $\mathbf{X}_p \in \mathbb{R}^{C \times N \times D}$.

$$\mathbf{X}_{p}^{'} = \operatorname{Patching}(X), \ \mathbf{X}_{p} = \operatorname{Embedding}(\mathbf{X}_{p}^{'})$$
 (1)

The Embedding (\cdot) operation transforms each patch from its original length P to a hidden dimension D through a trainable linear layer. In addition, we flatten the first two dimensions to obtain a set of spatial-temporal patches with

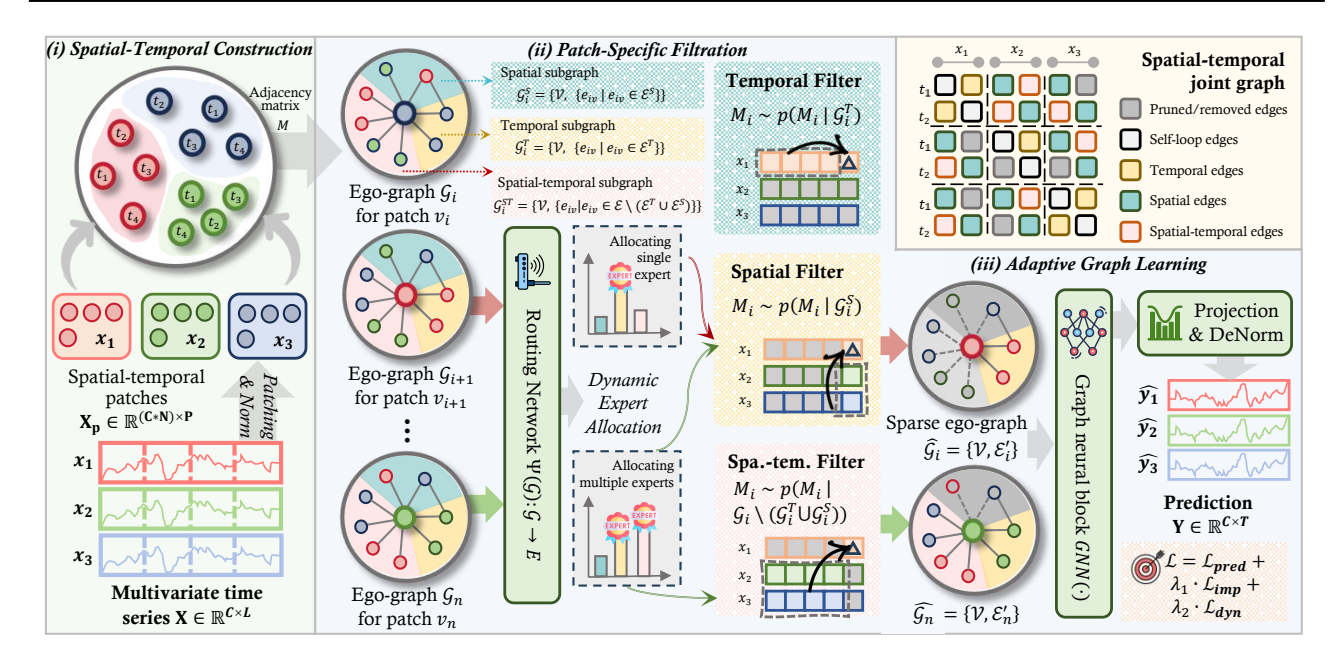


Figure 3. The overall structure of TimeFilter, which consists of: (i) **Spatial-Temporal Construction** is devised to construct the spatial-temporal graph from the input **X**; (ii) **Patch-Specific Filtration** facilitates spatial-temporal dependencies by filtering out irrelevant information for each patch; (iii) **Adaptive Graph Learning** is leveraged to predict the future **Y** based on GNN.

 $n = C \times N$ patches containing the enhanced local information $\mathbf{X}_p \in \mathbb{R}^{n \times D}$.

Next, we calculate the projection distances in a multi-head manner, allowing for richer similarity representation. We first divide \mathbf{X}_p into different heads $\mathbf{X}_h \in \mathbb{R}^{H \times n \times \lfloor \frac{D}{H} \rfloor}$ and then calculate the projection distances $\mathrm{Dist}(\cdot)$ by dot product. Here, H is the number of heads and A^T is the transpose.

$$Dist(\mathbf{X}_h) = Linear(\mathbf{X}_h) * Linear(\mathbf{X}_h)^T \in \mathbb{R}^{H \times n \times n}$$
(2)

Subsequently, based on above distances, we construct the graph with the k-Nearest Neighbor (k-NN) method. Each spatial-temporal patch is considered as a node, resulting in a total of n nodes. For each node, we retain the k nearest neighbors. In practice, we retain the $k = \lfloor \alpha * n \rfloor$ nearest neighbors, where α is a hand-tuned scaling factor. Formally, the adjacency matrix \mathbf{M} can formulated as follows

$$\mathbf{M} = k\text{-NN}(\text{GeLU}(\text{Dist}(\mathbf{X}_h)), \alpha) \tag{3}$$

Instead of using the whole graph \mathcal{G} with non-negligible noise (Huang et al., 2023), we decompose \mathcal{G} into n patch-specific ego graphs $\{\mathcal{G}_i\}_1^n$ to effectively resist noise, each corresponding to a patch. Each ego graph is further divided into three regions: temporal, spatial and spatial-temporal.

$$\mathcal{G}_i^T = \{ \mathcal{V}, \{ e_{iv} | e_{iv} \in \mathcal{E}_i^T \} \}$$

$$\tag{4}$$

$$\mathcal{G}_i^S = \{ \mathcal{V}, \{ e_{iv} | e_{iv} \in \mathcal{E}_i^S \} \}$$
 (5)

$$\mathcal{G}_i^{ST} = \{ \mathcal{V}, \{ e_{iv} | e_{iv} \in \mathcal{E} \setminus (\mathcal{E}^S \cup \mathcal{E}_i^T) \} \}$$
 (6)

Here \mathcal{E}_i^S is the spatial edge set, \mathcal{E}_i^T is the temporal edge set, e_v is one of the edges and $\forall i \in \{1,2,...,n\}$. The adjacency matrix of each subgraph \mathbf{M}_i can be obtained by applying different masks to \mathbf{M} .

With the above designs, we obtain n ego graphs G_i and the corresponding adjacency matrix M_i to represent the correlations of each patch.

4.2. Patch-Specific Filtration (PSF) Module

After constructing the graph, each edge connects two patch nodes, representing their dependency relationship. At this stage, we design a patch-specific MoE module composed of *routing network*, *dynamic expert allocation* and *filtration* to identify effective dependencies, filter out irrelevant ones, and obtain the spatial-temporal relationship.

Routing Network. We observe that time series data from different domains exhibit distinct characteristics and underlying structures, necessitating the modeling of different types of dependencies. Therefore, for each ego graph \mathcal{G}_i , we design three experts for different dependencies, including Temporal Filter, Spatial Filter, and Spa.-tem. Filter. Based on the router's decisions, filters with different dependency regions are assigned to different patches. Specifically, the filtration operation can be formulated as follows:

• **Temporal Filter** $\mathbf{M}_i \sim p(\mathbf{M}_i | \mathcal{G}_i^T)$ if the selection includes a Temporal Filter, the temporal edges \mathcal{E}^T are re-

tained. For example, user behavior data with low interchannel correlation benefits more from temporal dependencies (Yuan et al., 2022), which leverage the historical information of individual users.

- Spatial Filter $\mathbf{M}_i \sim p(\mathbf{M}_i | \mathcal{G}_i^S)$ If the selection includes a Spatial Filter, the spatial edges \mathcal{E}^S are retained. This can be crucial for scenarios where spatial dependencies reflect the synchronization between multiple variables in real-time monitoring.
- Spa.-tem. Filter: $\mathbf{M}_i \sim p(\mathbf{M}_i|\mathcal{G}_i^{ST})$ If the selection includes a Spatial-temporal Filter, the spatial edges $\mathcal{E}\setminus(\mathcal{E}^S\cup\mathcal{E}_i^T)$ are retained. For instance, in traffic flow prediction, spatial-temporal dependencies are pivotal (Wang et al., 2024b), capturing the nuanced interactions between traffic dynamics across different locations and their evolution over time.

Following the classic concept of a (sparsely-gated) mixture-of-experts (Shazeer et al., 2017b; Zhang et al., 2024a) and graph sparsification paradigms (Wang et al., 2024a; Zhang et al., 2024b;c), we calculate the confidence r of the current patch for each filter using a noisy gating mechanism.

$$r(\mathcal{G}_i) = \text{Softmax}(\psi(\mathbf{M}_i)),$$
 (7)

$$\psi(\mathbf{M}_i) = \operatorname{Linear}_q(\mathbf{M}_i) + \epsilon \cdot \operatorname{Softplus}(\operatorname{Linear}_n(\mathbf{M}_i))$$
 (8)

where $\psi(\mathbf{M}) \in \mathbb{R}^m$ is the calculated scores of patches for all filters, $\epsilon \in \mathcal{N}(0,1)$ is denotes the standard Gaussian noise, Linear_g and Linear_n are clean and noisy scores mapping, respectively. m is the number of filters and in TimeFilter m=3.

Dynamic Expert Allocation. The classical Top-K routing MoE architecture assumes that the same number of experts is assigned to each input token, but this overlooks the differences between inputs. Specifically, in dependency modeling, certain time patches require a different number of dependencies. For example, when there is a clear leadlag effect in stock data, both temporal and spatial-temporal dependencies are needed, while during unexpected events, spatial dependencies are more crucial to capture how stocks from the same sector react.

To adaptively customize the dependency relationships for each patch, we propose Dynamic Expert Allocation module to select filters based on the confidence of the patch itself, following MoE-Dynamic (Huang et al., 2024). Unlike the Top-K routing mechanism, which selects a fixed number of experts, our method allows the model to evaluate whether the current selection of dependencies is sufficient. If not, it will continue to allocate more dependencies.

Thus, we rank the confidence r from largest to smallest, resulting in a sorted index list I. Afterward, we find the

smallest set of filters whose cumulative probability exceeds the threshold Top-p, and the number of selected filters q is calculated by:

$$q(\mathcal{G}_i) = \operatorname*{arg\,min}_{j \in \{1, 2, \dots, m\}} \sum_{k < j} r(\mathcal{G}_i)_k \ge \text{Top-}p \tag{9}$$

Next, the calculation of output routing is:

$$g(\mathcal{G}_i)_j = \begin{cases} r(\mathcal{G}_i)_j, & \text{Filter}_j \in S_i \\ 0, & \text{Filter}_j \notin S_i \end{cases}, j \in \{1, 2, ..., m\}$$
 (10)

where S is the set of selected filters controlled by $q(G_i)$ in Eq. 9:

$$S_i = \{ \text{Filter}_{I_1}, \text{Filter}_{I_2}, ..., \text{Filter}_{I_{q(\mathcal{G}_i)}} \}$$
 (11)

Filtration. Finally, each ego graph \mathcal{G}_i , $\forall i \in \{1, 2, ..., n\}$, based on output dynamic routing $g(\mathcal{G}_i) \in \mathbb{R}^m$, we perform a filtration operation on \mathbf{M}_i to obtain the adjacency matrix \mathbf{M}_i' and the corresponding edge set \mathcal{E}_i' and the sparse graph $\widehat{\mathcal{G}}_i$ after filtering out redundant dependencies. For example, if $S_i = \{\text{Temporal Filter}, \text{Spa.-tem. Filter}\}$, the ego graph after filtering will be:

$$\widehat{\mathcal{G}}_i = \{ \mathcal{V}, \{ e_{iv} | e_{iv} \in \mathcal{E}_i^T \cup \mathcal{E} \setminus (\mathcal{E}^S \cup \mathcal{E}_i^T) \} \}$$
 (12)

It is worth noting that the filtration operation on the n egographs can be performed in parallel without introducing additional computational complexity.

4.3. Adaptive Graph Learning (AGL) Module

After obtaining $\widehat{\mathcal{G}}_i = \{\mathcal{V}, \mathcal{E}_i'\}$, we restore the n ego graphs into a global graph $\widehat{\mathcal{G}}$ and aggregate the \mathbf{M}_i' into corresponding \mathbf{M}' .

$$\widehat{\mathcal{G}} = \bigcup_{1}^{n} \widehat{\mathcal{G}}_{i} = \{ \mathcal{V}, \bigcup_{1}^{n} \mathcal{N}(v_{i}) \}$$
 (13)

where $\mathcal{N}(\cdot)$ is the set of neighboring nodes of a given node.

Then, the graph learning layer learns the graph adjacency matrix $\mathbf{M}^{'}$ adaptively to capture the hidden relationships among time series data.

$$h_i^{(l)} = \texttt{COMB}(h_i^{(l-1)}, \texttt{AGGR}\{h_j^{(k-1)}: v_j \in \mathcal{N}(v_i)\}) \ \ (14)$$

where $0 \leq l \leq O$, O is the number of GNN layers, $h_i^{(0)} = \mathbf{X}_h \in \mathbb{R}^{H \times n \times \lfloor \frac{D}{H} \rfloor}$ and $h_i^{(l)} (1 \leq l \leq O)$ is the embedding of node v_i at the l-th layer. AGGR (\cdot) and COMB (\cdot) are the functions used for aggregating neighborhood information and combining ego- and neighbor-representations, respectively. The AGGR (\cdot) employed in TimeFilter is an additive operation, where the representation of each node is updated by summing the features of its neighboring nodes.

Finally, to perform forecasting, our model utilizes a residual module and a linear projection in time dimension. This transformation can be expressed as:

$$\mathbf{Y} = \operatorname{Linear}(\mathbf{X}_h + h^{(O)}) \in \mathbb{R}^{C \times T}$$
 (15)

4.4. Loss Function

The loss function of TimeFilter consists of three components. For the predictors, the Mean Squared Error (MSE) loss $(\mathcal{L}_{pred} = \frac{1}{T} \sum_{i=0}^{T} \|\mathbf{x}_{:,i} - \hat{\mathbf{x}}_{:,i}\|_2^2)$ is used to measure the variance between predicted values and ground truth. Moreover, following dynamic routing (Huang et al., 2024), we introduce an dynamic loss \mathcal{L}_{dyn} to avoid assigning low confidence to all experts, thereby activating a larger number of experts to achieve better performance.

$$\mathcal{L}_{\text{dyn}} = -\frac{1}{n} \sum_{i=1}^{n} \sum_{j=1}^{m} r(\mathcal{G}_i)_j * \log(r(\mathcal{G}_i)_j)$$
 (16)

Moreover, we introduce an expert importance loss \mathcal{L}_{imp} (Shazeer et al., 2017a) to prevent TimeFilter from converging to a trivial solution where only a single group of experts is consistently selected:

$$\mathcal{L}_{imp} = \frac{1}{n} \sum_{i=1}^{n} \frac{Std(r(\mathcal{G}_i))}{Mean(r(\mathcal{G}_i)) + \epsilon}$$
(17)

where ϵ is a small positive constant to prevent numerical instability, $Std(\cdot)$ and $Mean(\cdot)$ calculate the standard deviation and the mean, respectively. Therefore, the final loss function is defined as:

$$\mathcal{L} = \mathcal{L}_{pred} + \lambda_1 \mathcal{L}_{dyn} + \lambda_2 \mathcal{L}_{imp}, \tag{18}$$

where λ_1 and λ_2 are the scaling factors.

5. Experiments

5.1. Experimental Setup

Datasets. For long-term forecasting, we conduct extensive experiments on selected 9 commonly real-world datasets from various application scenarios, including ETT (ETTh1, ETTh2, ETTm1, ETTm2), Traffic, Electricity, Weather, Solar-Energy (Miao et al., 2024a;b) and Climate (with 1763 channels) datasets. For short-term forecasting, we adopt 4 benchmarks from PEMS (PEMS03, PEMS04, PEMS07, PEMS08) (Liu et al., 2025b;a). The statistics of the dataset are shown in Appendix A.1.

Baselines. We compare our method with SOTA representative methods, including GNN-based methods: MS-GNet (Cai et al., 2024), CrossGNN (Huang et al., 2023); Transformer-based methods: CATS (Kim et al., 2024), iTransformer (Liu et al., 2024b), PatchTST (Nie et al., 2023), Crossformer (Zhang & Yan, 2023), FEDformer (Zhou et al., 2022); Linear-based methods: Leddam (Yu et al., 2024), SOFTS (Han et al., 2024a), DUET (Qiu et al., 2024b), DLinear (Zeng et al., 2023), TiDE (Das et al., 2023); CNN-based methods: ModernTCN (Donghao & Xue, 2024), Times-Net (Wu et al., 2023), SCINet (Liu et al., 2022). In addition,

CCM (Chen et al., 2024) is included as a plug-in in the baseline as PatchTST+CCM, or CCM for short.

Implementation Details. All experiments are implemented in PyTorch (Paszke et al., 2019) and conducted on one NVIDIA A100 40GB GPU. We use the Adam optimizer (Kingma, 2014) with a learning rate selected from $\{1e^{-3}, 1e^{-4}, 5e^{-4}\}$. The Top-p in dynamic expert allocation is selected from $\{0.0, 0.5\}$. We select two common metrics in time series forecasting: Mean Absolute Error (MAE) and Mean Squared Error (MSE). For additional details on hyperparameters and settings, please refer to Appendix A.3.

5.2. Results

Long-term Forecasting. We report the results of the long-term forecasting in Table 1. The input length L is 96 for our method and all baselines. The forecasting horizon T is $\{96,192,336,720\}$. The results show that TimeFilter adaptively models various dependencies for each dataset in different domains, and has been proven to yield significant improvements. Compared to the second-best model Leddam (Yu et al., 2024), TimeFilter reduces MSE and MAE by 4.48%/2.23%, respectively.

Additionally, we perform the Wilcoxon test with Leddam (Yu et al., 2024) and obtain the p-value of $4.66e^{-10}$, indicating a significant improvement at the 99% confidence level. The detailed error bars are shown in Appendix B.1.

Furthermore, according to the scaling law (Shi et al., 2024) of TSF, for a given dataset size, as the look-back horizon L increases, so does the noise in the input sequence, which does not necessarily improve the performance of the model. In addition, the dataset size has more influence on the optimal horizon, while the model size has less influence. Therefore, we conduct a search for different look-back horizons to determine the optimal horizon for the 4 relatively large datasets and compare TimeFilter with other baselines. As shown in Table 2, TimeFilter demonstrates robust resistance to noise and maintains SOTA performance even with longer optimal horizon inputs, outperforming other methods. Specifically, compared to the channel clustering strategy methods DUET (Qiu et al., 2024b) and CCM (Chen et al., 2024), TimeFilter reduces MSE and MAE by 5.34%/1.40%and 6.89%/3.69%, respectively. This demonstrates the effectiveness of our fine-grained adaptive filtration strategy.

Short-term Forecasting. We report the results of the short-term forecasting in Table 3. The input length L is 96 for our method and all baselines. The forecasting horizon T is $\{12, 24, 48\}$. From the table, TimeFilter consistently outperforms other methods across all 4 PEMS datasets. Specifically, on PEMS08, TimeFilter reduces MSE and MAE by 13.54%/3.13% compared to the second-best DUET (Qiu

Models		Filter urs)	DU CC (2	JET 2024b)		former 2024b)	Led CD (dam 2024)		GNet 2024)		FTS 24a)		sGNN 2023)	Patcl CI (2		Crossi	former 2023)		esNet 2023)	DLi CI (2			former (2022)
Metric	MSE	MAE	MSE	MAE	MSE	MAE	MSE	MAE	MSE	MAE	MSE	MAE	MSE	MAE	MSE	MAE	MSE	MAE	MSE	MAE	MSE	MAE	MSE	MAE
ETT (Avg.)	0.358	0.385	0.371	0.388	0.383	0.399	0.368	0.388	0.384	0.403	0.379	0.396	0.371	0.392	0.381	0.397	0.685	0.578	0.391	0.404	0.446	0.447	0.408	0.428
Weather	0.239	0.269	0.251	0.273	0.258	0.279	0.242	0.272	0.249	0.278	0.255	0.278	0.247	0.289	0.259	0.281	0.259	0.315	0.259	0.287	0.265	0.315	0.309	0.360
Electricity	0.158	0.256	0.172	0.258	0.178	0.270	0.169	0.263	0.194	0.300	0.174	0.264	0.201	0.300	0.216	0.304	0.244	0.334	0.193	0.295	0.225	0.319	0.214	0.327
Traffic	0.407	0.268	0.451	0.269	0.428	0.282	0.467	0.294	0.641	0.370	0.409	0.267	0.583	0.323	0.555	0.362	0.550	0.304	0.620	0.336	0.625	0.383	0.610	0.376
Solar-Energy	0.223	0.250	0.237	0.233	0.233	0.262	0.230	0.264	0.262	0.288	0.229	0.256	0.324	0.377	0.270	0.307	0.641	0.639	0.301	0.319	0.330	0.401	0.292	0.381

Table 1. Long-term forecasting results. The input length L is 96. All results are averaged across four different forecasting horizons: $T \in \{96, 192, 336, 720\}$. The best and second-best results are in **bold** and <u>underlined</u>, respectively. See Table 8 for full results.

Models	Time (Or	Filter urs)	DU CC (2		CC (2		PI CI (2	OF 2024)	111000	rnTCN 2024)	iTrans		CA CD (2		Patch CI (2		Cross	former 2023)	Time CD (esNet 2023)		near 2023)
Metric	MSE	MAE	MSE	MAE	MSE	MAE	MSE	MAE	MSE	MAE	MSE	MAE	MSE	MAE	MSE	MAE	MSE	MAE	MSE	MAE	MSE	MAE
Weather	0.216	0.258	0.218	0.252	0.225	0.263	0.225	0.261	0.224	0.264	0.232	0.270	0.244	0.272	0.226	0.264	0.234	0.292	0.255	0.282	0.242	0.293
Electricity	0.150	0.246	0.158	0.248	0.167	0.261	0.156	0.250	0.156	0.253	0.163	0.258	0.178	0.264	0.159	0.253	0.181	0.279	0.192	0.295	0.166	0.264
Traffic	0.360	0.254	0.394	0.257	0.389	0.259	0.377	0.256	0.396	0.270	0.397	0.281	0.449	0.283	0.391	0.264	0.523	0.284	0.620	0.336	0.434	0.295
Climate	1.047	0.490	1.103	0.509	1.123	0.512	1.315	0.555	1.155	0.542	1.060	0.496	1.095	0.509	1.387	0.562	1.170	0.550	1.295	0.569	1.134	0.541

Table 2. Long-term forecasting results. The input length L is searched from $\{192, 336, 512, 720\}$ for optimal horizon in the scaling law of TSF (Shi et al., 2024). All results are averaged across four different forecasting horizons: $T \in \{96, 192, 336, 720\}$. The best and second-best results are in **bold** and underlined, respectively. See Table 9 for full results.

Models		Filter ırs)	DU CC (2		iTrans CD (2	former 2024b)	Led CD (dam 2024)		FTS 24a)		hTST 2023)	Crossi CD (former 2023)	Time CD (esNet 2023)		DE 2023)	DLi CI (2	near 2023)		Net 2022)		cormer (2022)
Metric	MSE	MAE	MSE	MAE	MSE	MAE	MSE	MAE	MSE	MAE	MSE	MAE	MSE	MAE	MSE	MAE	MSE	MAE	MSE	MAE	MSE	MAE	MSE	MAE
PEMS03	0.084	0.191	0.086	0.192	0.096	0.204	0.101	0.210	0.087	0.192	0.151	0.265	0.138	0.253	0.119	0.271	0.271	0.380	0.219	0.295	0.093	0.203	0.167	0.291
PEMS04	0.083	0.186	0.096	0.203	0.098	0.207	0.102	0.213	0.091	0.196	0.162	0.273	0.145	0.267	0.109	0.220	0.307	0.405	0.236	0.350	0.085	0.194	0.195	0.308
PEMS07	0.071	0.170	0.076	0.176	0.088	0.190	0.087	0.192	0.075	0.173	0.166	0.270	0.181	0.272	0.106	0.208	0.297	0.394	0.241	0.343	0.112	0.211	0.133	0.282
PEMS08	0.083	0.186	0.096	0.192	0.127	0.212	0.102	0.211	0.114	0.208	0.238	0.289	0.232	0.270	0.150	0.244	0.347	0.421	0.281	0.366	0.133	0.225	0.234	0.326

Table 3. Short-term forecasting results. The input length L is 96. All results are averaged across three different forecasting horizons: $T \in \{12, 24, 48\}$. The best and second-best results are in **bold** and underlined, respectively. See Table 10 for full results.

et al., 2024b). On PEMS07 with 883 channels, TimeFilter reduces MSE and MAE by 5.33%/1.73% compared to the second-best SOFTS (Han et al., 2024a).

5.3. Ablation Study

To validate the effectiveness of TimeFilter, we conduct a comprehensive ablation study on its architectural design.

Comparison of different Filter methods. We carefully design six other filtering methods and the comparison is shown in the Filter Replace section of Table 4. **Top-**K strategy selects the top K edges with the largest weights from the ego graph \mathcal{G}_i of each patch, while **Random-**K randomly selects K edges. **RegionTop-**K strategy selects the top K edges with the largest weights within the region corresponding to three types of dependencies, while **RegionThre** learns a threshold for each region through a linear mapping and selects edges with weights greater than the threshold in each region. **C-Filter** refers to channel-wise filtering, where

all patches within the look-back sequence are filtered based on the same type of dependency. The **w/o Filter** refers to the case where no filtering is applied after graph construction.

The result shows that TimeFilter consistently outperforms other filtering methods. We conclude that higher-weight relationships may be due to spurious regression (Liu et al., 2024a) rather than effective dependencies. Furthermore, time series data from different domains require different types of relationships.

MoE component ablation. We conduct an ablation study on the routing mechanism (Static Routing with only the most significant filter selected) and $\mathcal{L}_{imp \& dyn}$, demonstrating the importance of dynamic selection and load balancing.

5.4. Model Analysis

Case study on dependency modeling. As shown in Figure 4, we visualize the dependencies and distribution of

Catagories	1						Filter F	Replace							1	Mo	ÞΕ	
Cases	Time	Filter	Top	o- <i>K</i>	Rando	om-K	Region	Top-K	Regio	nThre	C-F	ilter	w/o I	Filter	Static F	Routing	w/o ∠ i	mp & dyn
	MSE	MAE	MSE	MAE	MSE	MAE	MSE	MAE	MSE	MAE	MSE	MAE	MSE	MAE	MSE	MAE	MSE	MAE
Weahter	0.239	0.269	0.243	0.272	0.243	0.272	0.241	0.271	0.241	0.270	0.242	0.271	0.244	0.273	0.242	0.271	0.243	0.272
Electricity	0.158	0.256	0.167	0.263	0.168	0.264	0.168	0.263 0	0.172	0.267	0.170	0.265	0.167	0.263	0.164	0.260	0.163	0.259
Traffic	0.407	0.268	0.413	0.271	0.412	0.271	0.411	0.270	0.412	0.271	0.413	0.271	0.414	0.273	0.410	0.271	0.410	0.271
Solar	0.223	0.250	0.231	0.258	0.231	0.258	0.233	0.257	0.235	0.259	0.234	0.258	0.234	0.262	0.228	0.258	0.227	0.258
ETTh1	0.426	0.431	0.441	0.438	0.441	0.437	0.441	0.438 0	0.437	0.436	0.431	0.436	0.442	0.438	0.440	0.434	0.430	0.432
ETTm2	0.272	0.321	0.276	0.324	0.276	0.323	0.273	0.323 0	0.276	0.324	0.277	0.325	0.277	0.324	0.274	0.322	0.273	0.322
PEMS08	0.083	0.186	0.086	0.191	0.085	0.189	0.085	0.190 0	0.085	0.189	0.086	0.190	0.086	0.191	0.084	0.188	0.084	0.187

Table 4. Ablation study of TimeFilter. The The input length L is 96. See Table 11 for full results.

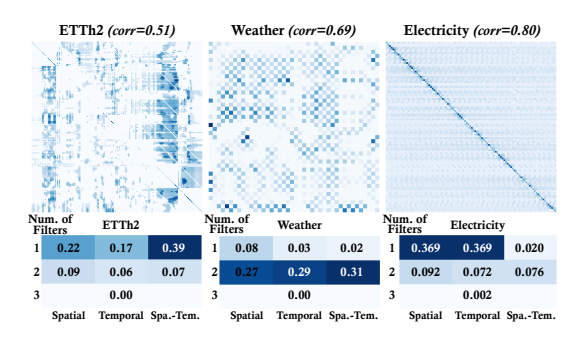


Figure 4. Above are the dependencies learned by TimeFilter from the ETTh2, Weather and Electricity datasets. Below is the distribution of selected filters, where the x-axis represents the dependency types and the y-axis represents the number of different filters.

selected filters of one batch in the ETTh2, Weather, and Electricity datasets. Indeed, it shows that different datasets require different types of dependency and that TimeFilter can capture these dependencies powerfully. Furthermore, as the correlation (Qiu et al., 2024a) within datasets increases, TimeFilter tends to utilize more effective dependencies to capture future variations. TimeFilter customizes the filtering of redundant dependencies for each dataset, enhancing its ability to express omni-series representations.

Influence of look-back horizon. To find the optimal horizon (Shi et al., 2024), we explore how varying the length of look-back horizons from $\{48, 96, 192, 336, 512, 720\}$ impacts the forecasting performance. As shown in Figure 5, TimeFilter effectively resists noise and exploits vital information in longer sequences, outperforming other models over different look-back horizons. Furthermore, as the hyperparameter length of the patch P increases proportionally with the look-back horizon L, the memory usage and inference efficiency of TimeFilter remain almost unchanged, thus preventing memory explosion in extremely long sequences.

Efficiency Analysis. We comprehensively compare the forecasting performance, training speed, and memory footprint of TimeFilter and other baselines, using the official

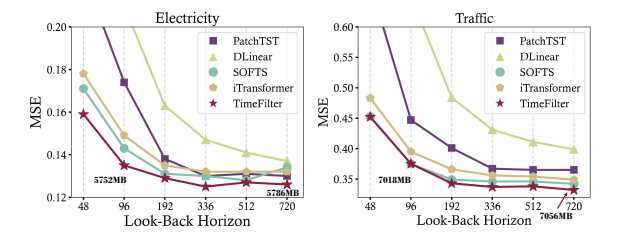


Figure 5. Influence of look-back horizon. TimeFilter consistently outperforms other models under different look-back horizons.

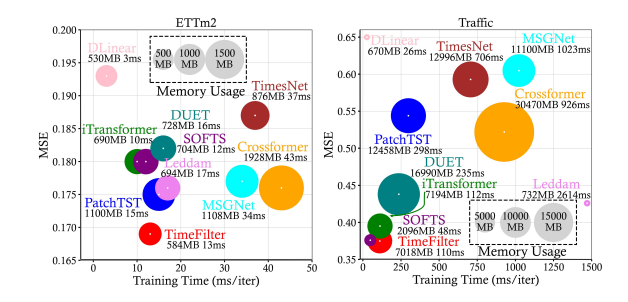


Figure 6. Model efficiency comparison under input-96-predict-96 of ETTm2 and Traffic datasets.

model configurations and the same batch size. As shown in Figure 6, the efficiency of TimeFilter exceeds other Transformer-based, CNN-based and GNN-based methods.

6. Conclusion

Considering the complex dynamic interactions inherent in real-world multivariate time series, we propose TimeFilter to adaptively, finely, and robustly model the dependencies. Technically, we design patch-specific filtration to effectively remove redundant relationships, thereby exploiting the most important dependencies for accurate forecasting. Extensive experiments show that TimeFilter consistently achieves SOTA performance in both long- and short-term forecasting tasks. Our work provides an in-depth exploration of dependency modeling in TSF, which we believe may pave the way for further research into dependency representations.

Acknowledgements

Dai Tao is supported in part by the National Natural Science Foundation of China, under Grant (62302309, 62171248), Shenzhen Science and Technology Program (JCYJ20220818101014030, JCYJ20220818101012025).

Impact Statement

Time series forecasting plays a crucial role in a variety of real-world domains, such as finance, weather forecasting, and traffic control. Our study presents a novel method for enhancing the dependency modeling. The datasets utilized are publicly accessible, promoting transparency and reproducibility. We do not anticipate any ethical issues arising from this work. The primary contributions of this research advance the field of time series forecasting, with potential applications in multiple sectors.

References

- Cai, W., Liang, Y., Liu, X., Feng, J., and Wu, Y. Msgnet: Learning multi-scale inter-series correlations for multivariate time series forecasting. *Proceedings of the AAAI Conference on Artificial Intelligence*, 2024.
- Chen, J., Lenssen, J. E., Feng, A., Hu, W., Fey, M., Tassiulas, L., Leskovec, J., and Ying, R. From similarity to superiority: Channel clustering for time series forecasting. *Advances in Neural Information Processing Systems*, 2024.
- Dai, T., Wu, B., Liu, P., Li, N., Bao, J., Jiang, Y., and Xia, S.-T. Periodicity decoupling framework for long-term series forecasting. *International Conference on Learning Representations*, 2024.
- Das, A., Kong, W., Leach, A., Sen, R., and Yu, R. Longterm forecasting with tiDE: Time-series dense encoder. *arXiv preprint arXiv:2304.08424*, 2023.
- Donghao, L. and Xue, W. ModernTCN: A modern pure convolution structure for general time series analysis. *International Conference on Learning Representations*, 2024.
- Godahewa, R., Bergmeir, C., Webb, G. I., Hyndman, R. J., and Montero-Manso, P. Monash time series forecasting archive. *arXiv* preprint arXiv:2105.06643, 2021.
- Han, L., Chen, X.-Y., Ye, H.-J., and Zhan, D.-C. SOFTS: Efficient multivariate time series forecasting with seriescore fusion. In *Advances in Neural Information Process*ing Systems, 2024a.
- Han, L., Ye, H.-J., and Zhan, D.-C. The capacity and robustness trade-off: Revisiting the channel independent strategy for multivariate time series forecasting. *IEEE Trans. on Knowl. and Data Eng.*, pp. 7129–7142, 2024b.

- Hu, Y., Liu, P., Zhu, P., Cheng, D., and Dai, T. Adaptive multi-scale decomposition framework for time series forecasting. *arXiv preprint arXiv:2406.03751*, 2024.
- Huang, Q., Shen, L., Zhang, R., Ding, S., Wang, B., Zhou, Z., and Wang, Y. CrossGNN: Confronting noisy multivariate time series via cross interaction refinement. In Advances in Neural Information Processing Systems, 2023.
- Huang, Q., An, Z., Zhuang, N., Tao, M., Zhang, C., Jin, Y., Xu, K., Xu, K., Chen, L., Huang, S., and Feng, Y.
 Harder task needs more experts: Dynamic routing in MoE models. In *Proceedings of the 62nd Annual Meeting of the Association for Computational Linguistics (Volume 1: Long Papers)*. Association for Computational Linguistics, August 2024.
- Karevan, Z. and Suykens, J. A. Transductive lstm for timeseries prediction: An application to weather forecasting. *Neural Networks*, 125:1–9, 2020.
- Kim, D., Park, J., Lee, J., and Kim, H. Are self-attentions effective for time series forecasting? *Advances in Neural Information Processing Systems*, 2024.
- Kingma, D. P. Adam: A method for stochastic optimization. *arXiv preprint arXiv:1412.6980*, 2014.
- Lai, G., Chang, W.-C., Yang, Y., and Liu, H. Modeling long-and short-term temporal patterns with deep neural networks. In *International ACM SIGIR conference on research & development in information retrieval*, pp. 95–104, 2018.
- Lin, S., Lin, W., Wu, W., Zhao, F., Mo, R., and Zhang, H. Segrnn: Segment recurrent neural network for long-term time series forecasting. *arXiv preprint arXiv:2308.11200*, 2023.
- Lin, S., Lin, W., Wu, W., Chen, H., and Yang, J. Sparsetsf: Modeling long-term time series forecasting with 1k parameters. *International Conference on Machine Learning*, 2024.
- Liu, C., Miao, H., Xu, Q., Zhou, S., Long, C., Zhao, Y., Li, Z., and Zhao, R. Efficient multivariate time series forecasting via calibrated language models with privileged knowledge distillation. In *ICDE*, 2025a.
- Liu, C., Xu, Q., Miao, H., Yang, S., Zhang, L., Long, C., Li, Z., and Zhao, R. Timecma: Towards llm-empowered multivariate time series forecasting via cross-modality alignment. In *AAAI*, volume 39, pp. 18780–18788, 2025b.
- Liu, M., Zeng, A., Chen, M., Xu, Z., Lai, Q., Ma, L., and Xu, Q. SCInet: Time series modeling and forecasting with sample convolution and interaction. *Advances in Neural Information Processing Systems*, 35:5816–5828, 2022.

- Liu, P., Wu, B., Hu, Y., Li, N., Dai, T., Bao, J., and Xia, S.-T. Timebridge: Non-stationarity matters for long-term time series forecasting. *arXiv preprint arXiv:2410.04442*, 2024a.
- Liu, Y., Hu, T., Zhang, H., Wu, H., Wang, S., Ma, L., and Long, M. iTransformer: Inverted transformers are effective for time series forecasting. *International Conference* on *Learning Representations*, 2024b.
- Miao, H., Liu, Z., Zhao, Y., Guo, C., Yang, B., Zheng, K., and Jensen, C. S. Less is more: Efficient time series dataset condensation via two-fold modal matching. *PVLDB*, 18(2):226–238, 2024a.
- Miao, H., Zhao, Y., Guo, C., Yang, B., Zheng, K., Huang, F., Xie, J., and Jensen, C. S. A unified replay-based continuous learning framework for spatio-temporal prediction on streaming data. In *ICDE*, pp. 1050–1062, 2024b.
- Morid, M. A., Sheng, O. R. L., and Dunbar, J. Time series prediction using deep learning methods in healthcare. *ACM Trans. Manage. Inf. Syst.*, 14, 2023.
- Nie, Y., H. Nguyen, N., Sinthong, P., and Kalagnanam, J. A time series is worth 64 words: Long-term forecasting with transformers. In *International Conference on Learning Representations*, 2023.
- Paszke, A., Gross, S., Massa, F., Lerer, A., Bradbury, J., Chanan, G., Killeen, T., Lin, Z., Gimelshein, N., Antiga, L., et al. Pytorch: An imperative style, high-performance deep learning library. *Advances in Neural Information Processing Systems*, 32, 2019.
- Qiu, X., Hu, J., Zhou, L., Wu, X., Du, J., Zhang, B., Guo, C., Zhou, A., Jensen, C. S., Sheng, Z., and Yang, B. Tfb: Towards comprehensive and fair benchmarking of time series forecasting methods. *Proc. VLDB Endow.*, 2024a.
- Qiu, X., Wu, X., Lin, Y., Guo, C., Hu, J., and Yang, B. Duet: Dual clustering enhanced multivariate time series forecasting. *arXiv preprint arXiv:2412.10859*, 2024b.
- Shazeer, N., Mirhoseini, A., Maziarz, K., Davis, A., Le, Q., Hinton, G., and Dean, J. Outrageously large neural networks: The sparsely-gated mixture-of-experts layer. In *International Conference on Learning Representations*, 2017a.
- Shazeer, N., Mirhoseini, A., Maziarz, K., Davis, A., Le, Q., Hinton, G., and Dean, J. Outrageously large neural networks: The sparsely-gated mixture-of-experts layer. In *International Conference on Learning Representations*, 2017b.
- Shi, J., Ma, Q., Ma, H., and Li, L. Scaling law for time series forecasting. *Advances in Neural Information Processing Systems*, 2024.

- Shu, W., Cai, K., and Xiong, N. N. A short-term traffic flow prediction model based on an improved gate recurrent unit neural network. *IEEE Transactions on Intelligent Transportation Systems*, 23(9):16654–16665, 2021.
- Volkovs, K., Urtans, E., and Caune, V. Primed unet-lstm for weather forecasting. In *Proceedings of the International Conference on Advances in Artificial Intelligence*, ICAAI '23, pp. 13–17, New York, NY, USA, 2024. Association for Computing Machinery. ISBN 9798400708985. doi: 10.1145/3633598.3633601.
- Wang, K., Li, G., Wang, S., Zhang, G., Wang, K., You, Y., Fang, J., Peng, X., Liang, Y., and Wang, Y. The snowflake hypothesis: Training and powering gnn with one node one receptive field. In *Proceedings of the 30th ACM SIGKDD Conference on Knowledge Discovery and Data Mining*, KDD '24, pp. 3152–3163, New York, NY, USA, 2024a. Association for Computing Machinery. ISBN 9798400704901. doi: 10.1145/3637528.3671766. URL https://doi.org/10.1145/3637528.3671766.
- Wang, Y., Xu, Y., Yang, J., Wu, M., Li, X., Xie, L., and Chen, Z. Fully-connected spatial-temporal graph for multivariate time-series data. *Proceedings of the AAAI Conference on Artificial Intelligence*, 2024b.
- Wu, H., Hu, T., Liu, Y., Zhou, H., Wang, J., and Long, M. TimesNet: Temporal 2d-variation modeling for general time series analysis. In *International Conference on Learning Representations*, 2023.
- Wu, Z., Pan, S., Long, G., Jiang, J., Chang, X., and Zhang, C. Connecting the dots: Multivariate time series forecasting with graph neural networks. In *Proceedings of the 26th* ACM SIGKDD International Conference on Knowledge Discovery & Data Mining, 2020.
- Yu, G., Zou, J., Hu, X., Aviles-Rivero, A. I., Qin, J., and Wang, S. Revitalizing multivariate time series forecasting: Learnable decomposition with inter-series dependencies and intra-series variations modeling. In Forty-first International Conference on Machine Learning, 2024.
- Yuan, E., Guo, W., He, Z., Guo, H., Liu, C., and Tang, R. Multi-behavior sequential transformer recommender. In Proceedings of the 45th International ACM SIGIR Conference on Research and Development in Information Retrieval, SIGIR '22. Association for Computing Machinery, 2022.
- Zeng, A., Chen, M., Zhang, L., and Xu, Q. Are transformers effective for time series forecasting? In *Proceedings of the AAAI conference on artificial intelligence*, volume 37, pp. 11121–11128, 2023.

- Zhang, G., Sun, X., Yue, Y., Jiang, C., Wang, K., Chen, T., and Pan, S. Graph sparsification via mixture of graphs. *arXiv* preprint arXiv:2405.14260, 2024a.
- Zhang, G., Wang, K., Huang, W., Yue, Y., Wang, Y., Zimmermann, R., Zhou, A., Cheng, D., Zeng, J., and Liang, Y. Graph lottery ticket automated. In *The Twelfth International Conference on Learning Representations*, 2024b. URL https://openreview.net/forum?id=nmBjBZoySX.
- Zhang, G., Yue, Y., Wang, K., Fang, J., Sui, Y., Wang, K., Liang, Y., Cheng, D., Pan, S., and Chen, T. Two heads are better than one: Boosting graph sparse training via semantic and topological awareness. *arXiv* preprint *arXiv*:2402.01242, 2024c.
- Zhang, Y. and Yan, J. Crossformer: Transformer utilizing cross-dimension dependency for multivariate time series forecasting. In *International Conference on Learning Representations*, 2023.
- Zhao, L. and Shen, Y. Rethinking channel dependence for multivariate time series forecasting: Learning from leading indicators. In *The Twelfth International Conference* on Learning Representations, 2024.
- Zhou, H., Zhang, S., Peng, J., Zhang, S., Li, J., Xiong, H., and Zhang, W. Informer: Beyond efficient transformer for long sequence time-series forecasting. In *Proceedings of the AAAI conference on artificial intelligence*, volume 35, pp. 11106–11115, 2021.
- Zhou, T., Ma, Z., Wen, Q., Wang, X., Sun, L., and Jin, R. FEDformer: Frequency enhanced decomposed transformer for long-term series forecasting. In *International Conference on Machine Learning*, pp. 27268–27286. PMLR, 2022.
- Zhu, P., Li, Y., Hu, Y., Liu, Q., Cheng, D., and Liang, Y. Lsr-igru: Stock trend prediction based on long short-term relationships and improved gru. *International Conference on Information and Knowledge Management*, 2024a.
- Zhu, P., Li, Y., Hu, Y., Xiang, S., Liu, Q., Cheng, D., and Liang, Y. Mci-gru: Stock prediction model based on multi-head cross-attention and improved gru. *arXiv* preprint arXiv:2410.20679, 2024b.

A. Implementation Details

A.1. Datasets

We conduct extensive experiments on eight widely-used time series datasets for long-term forecasting and PEMS datasets for short-term forecasting. We report the statistics in Table 5. Detailed descriptions of these datasets are as follows:

- (1) **ETT** (Electricity Transformer Temperature) dataset (Zhou et al., 2021) encompasses temperature and power load data from electricity transformers in two regions of China, spanning from 2016 to 2018. This dataset has two granularity levels: ETTh (hourly) and ETTm (15 minutes).
- (2) **Weather** dataset (Wu et al., 2023) captures 21 distinct meteorological indicators in Germany, meticulously recorded at 10-minute intervals throughout 2020. Key indicators in this dataset include air temperature, visibility, among others, offering a comprehensive view of the weather dynamics.
- (3) **Electricity** dataset (Wu et al., 2023) features hourly electricity consumption records in kilowatt-hours (kWh) for 321 clients. Sourced from the UCL Machine Learning Repository, this dataset covers the period from 2012 to 2014, providing valuable insights into consumer electricity usage patterns.
- (4) **Traffic** dataset (Wu et al., 2023) includes data on hourly road occupancy rates, gathered by 862 detectors across the freeways of the San Francisco Bay area. This dataset, covering the years 2015 to 2016, offers a detailed snapshot of traffic flow and congestion.
- (5) **Solar-Energy** dataset (Lai et al., 2018) contains solar power production data recorded every 10 minutes throughout 2006 from 137 photovoltaic (PV) plants in Alabama.
- (6) Climate dataset (Godahewa et al., 2021) records regional precipitation data across 1,763 stations in Australia.
- (7) **PEMS** dataset (Liu et al., 2022) comprises four public traffic network datasets (PEMS03, PEMS04, PEMS07, and PEMS08), constructed from the Caltrans Performance Measurement System (PeMS) across four districts in California. The data is aggregated into 5-minute intervals, resulting in 12 data points per hour and 288 data points per day.

Tasks	Dataset	Dim	Prediction Length	Dataset Size	Frequency
	ETTm1	7	{96, 192, 336, 720}	(34465, 11521, 11521)	15 min
	ETTm2	7	{96, 192, 336, 720}	(34465, 11521, 11521)	15 min
	ETTh1	7	{96, 192, 336, 720}	(8545, 2881, 2881)	15 min
Long-term	ETTh2	7	{96, 192, 336, 720}	(8545, 2881, 2881)	15 min
Forecasting	Weather	21	{96, 192, 336, 720}	(36792, 5271, 10540)	10 min
	Electricity	321	{96, 192, 336, 720}	(18317, 2633, 5261)	1 hour
	Traffic	862	{96, 192, 336, 720}	(12185, 1757, 3509)	1 hour
	Solar-Energy	137	{96, 192, 336, 720}	(36601, 5161, 10417)	10 min
	Climate	1763	{96, 192, 336, 720}	(6763, 989, 2070)	10 min
	PEMS03	358	12	(15617, 5135, 5135)	5 min
Short-term	PEMS04	307	12	(10172, 3375, 3375)	5 min
Forecasting	PEMS07	883	12	(16911, 5622, 5622)	5 min
	PEMS08	170	12	(10690, 3548, 265)	5 min

Table 5. Dataset detailed descriptions. "Dataset Size" denotes the total number of time points in (Train, Validation, Test) split respectively. "Prediction Length" denotes the future time points to be predicted. "Frequency" denotes the sampling interval of time points.

A.2. Metric Details

Regarding metrics, we utilize the mean square error (MSE) and mean absolute error (MAE) for long-term forecasting. The calculations of these metrics are:

$$MSE = \frac{1}{T} \sum_{i=0}^{T} (\hat{y}_i - y_i)^2, \qquad MAE = \frac{1}{T} \sum_{i=0}^{T} |\hat{y}_i - y_i|$$

A.3. Experiment details

All experiments are implemented in PyTorch (Paszke et al., 2019) and conducted on an NVIDIA A100 40GB GPU. We use the Adam optimizer (Kingma, 2014). The batch size is set to 16 for the Electricity and Traffic datasets, and 32 for all other datasets. Table 6 provides detailed hyperparameter settings for each dataset.

Tasks	Dataset	Length of Patch	e_layers	lr	d_model	d_ff	Num. of Epochs
	ETTm1	8	2	1e-4	256	256	10
	ETTm2	16	2	1e-4	128	128	10
	ETTh1	2	2	1e-4	128	256	10
Long-term	ETTh2	4	1	1e-4	128	256	10
Forecasting	Weather	48	2	5e-4	128	256	10
	Electricity	32	2	1e-3	512	512	15
	Traffic	96	3	1e-3	512	2048	30
	Solar-Energy	48	2	5e-4	256	512	10
	PEMS03	48	2	1e-3	512	1024	20
Short-term	PEMS04	48	2	5e-4	512	1024	20
Forecasting	PEMS07	96	2	1e-3	512	1024	20
	PEMS08	48	2	1e-3	512	512	20

Table 6. Hyperparameter settings for different datasets. "e_layers" denotes the number of graph block. "lr" denotes the learning rate. "d_model" and "d_ff" denote the model dimension of attention layers and feed-forward layers, respectively.

B. Full Results

B.1. Error Bars

In this paper, we repeat all the experiments three times. Here we report the standard deviation of our proposed TimeFilter and the second best model Leddam (Yu et al., 2024), as well as the statistical significance test in Table 7. We perform the Wilcoxon test with Leddam (Yu et al., 2024) and obtain the p-value of $4.66e^{-10}$, indicating a significant improvement at the 99% confidence level.

B.2. Long-term Forecasting

Table 8 and Table 9 present the full results for long-term forecasting, including both the results for the fixed look-back horizon L=96 results and the results obtained through hyperparameter search for the optimal horizon according to the scaling law (Shi et al., 2024) of TSF. The hyperparameter search process involved exploring look-back horizons $L \in \{192, 336, 512, 720\}$. In both settings, TimeFilter consistently achieves the best performance, demonstrating its effectiveness and robustness. In particular, under the optimal horizon condition, TimeFilter can still adaptively model effective dependencies in long sequences.

B.3. Short-term Forecasting

Table 10 present the full results for short-term forecasting. The look-back horizon L is set to 96 and the forecasting horizon $T \in \{12, 24, 48\}$. Across all four PEMS datasets, TimeFilter consistently delivers the highest performance, particularly with a significant improvement on PEMS08, showcasing its effectiveness and reliability.

Model	Time	Filter	Leddan	n (2024)	Confidence
Dataset	MSE	MAE	MSE	MAE	Interval
ETTm1	0.377 ± 0.004	0.393 ± 0.006	0.386 ± 0.008	0.397 ± 0.006	99%
ETTm2	0.272 ± 0.004	0.321 ± 0.002	0.281 ± 0.003	0.325 ± 0.003	99%
ETTh1	0.420 ± 0.005	0.428 ± 0.003	0.431 ± 0.005	0.429 ± 0.004	99%
ETTh2	0.364 ± 0.003	0.397 ± 0.002	0.373 ± 0.009	0.399 ± 0.007	99%
Weather	0.239 ± 0.006	0.269 ± 0.004	0.242 ± 0.009	0.272 ± 0.006	99%
Electricity	0.158 ± 0.005	0.256 ± 0.006	0.169 ± 0.005	0.263 ± 0.005	99%
Traffic	0.407 ± 0.008	0.268 ± 0.004	0.467 ± 0.006	0.294 ± 0.008	99%
Solar	0.223 ± 0.006	0.250 ± 0.003	0.230 ± 0.008	0.264 ± 0.005	99%

Table 7. Standard deviation and statistical tests for TimeFilter and second-best method (Leddam) on ETT, Weather, Electricity, Traffic, and Solar datasets.

B.4. Ablation Study

We present the full results of the ablation studies discussed in the main text in Table 11. We carefully design six other filtering methods to validate the effectiveness of TimeFilter.

- (1) **Top-**K strategy selects the top K edges with the largest weights from the ego graph \mathcal{G}_i of each patch.
- (2) **Random-**K randomly selects K edges from the ego graph G_i of each patch.
- (3) **RegionTop-**K strategy selects the top K edges with the largest weights within the region corresponding to three types of dependencies.
- (4) **RegionThre** learns a threshold for each region through a linear mapping and selects edges with weights greater than the threshold in each region.
- (5) **C-Filter** refers to channel-wise filtering, where all patches within the look-back sequence are filtered based on the same type of dependency.
- (6) w/o Filter refers to the case where no filtering is applied after graph construction.

C. Visualization

In order to facilitate a clear comparison between different models, we present supplementary prediction examples for four representative datasets, as Electricity in Figure 7, Traffic in Figure 8, Weather in Figure 9 and PEMS08 in Figure 10, respectively. The look-back horizon L is 96 for all four datasets. The forecasting horizon T is 96 for Eleltricity, Traffic and Weather, while T is 48 for PEMS08. Among the different models, TimeFilter delivers the most accurate predictions of future series variations and demonstrates superior performance.

Mo	odels		Filter urs)		JET 24b)		former 24b)	Led (20	dam (24)	MSC (20		SOI (20)	FTS 24a)	Cross			nTST (23)	Crossi		Time		DLi (20	near (23)		ormer
M	etric	MSE	MAE	MSE	MAE	MSE	MAE	MSE	MAE	MSE	MAE	MSE	MAE	MSE	MAE	MSE	MAE	MSE	MAE	MSE	MAE	MSE	MAE	MSE	MAE
ETTm1	96 192 336 720	0.356 0.386	0.402	$0.369 \\ 0.404$		0.377 0.426		0.394	0.383 0.402	0.417	$0.397 \\ 0.422$		$0.389 \\ 0.412$		$0.390 \\ 0.411$	$\frac{0.367}{0.399}$	0.385 0.410	0.532	0.451 0.515		$0.387 \\ 0.411$		$0.391 \\ 0.415$		0.441 0.459
	Avg.	0.377	0.393	0.390	0.393	0.407	0.410	0.386	0.397	0.398	0.411	0.393	0.403	0.393	0.404	0.387	0.400	0.513	0.496	0.400	0.406	0.404	0.408	0.448	0.452
ETTm2	96 192 336 720	0.235 0.293	0.336	0.243 0.304	$\frac{0.302}{0.341}$	0.250 0.311	0.264 0.309 0.348 0.407	0.243 0.303	0.303 0.341	$0.247 \\ 0.312$	$0.307 \\ 0.346$	0.246 0.319	$0.306 \\ 0.352$	0.240 0.304	$0.307 \\ 0.345$	0.241 0.305	$\begin{array}{c} \underline{0.302} \\ 0.343 \end{array}$	0.414 0.597	0.492 0.542	$0.249 \\ 0.321$	$0.309 \\ 0.351$	0.284 0.382	$0.361 \\ 0.429$	0.269 0.325	0.328 0.366
	Avg.	0.272	0.321	0.280	0.324	0.288	0.332	0.281	0.325	0.288	0.330	0.287	0.330	0.282	0.330	0.281	0.326	0.757	0.610	0.291	0.333	0.354	0.402	0.305	0.349
ETTh1		0.413 0.450	0.420 0.440	$0.429 \\ 0.471$	$0.425 \\ 0.446$	0.441 0.487	0.405 0.436 0.458 0.491	0.424 <u>0.459</u>	$\frac{0.422}{0.442}$	$0.442 \\ 0.480$	$0.442 \\ 0.468$	0.435 0.480	$0.431 \\ 0.452$	0.427 0.465	$0.425 \\ 0.445$	0.460 0.501	$0.445 \\ 0.466$	$0.471 \\ 0.570$	0.474 0.546	$0.436 \\ 0.491$	$0.429 \\ 0.469$	0.446 0.489	$0.441 \\ 0.467$	$\frac{0.420}{0.459}$	0.448 0.465
	Avg.	0.420	0.428	0.443	0.436	0.454	0.447	<u>0.431</u>	0.429	0.452	0.452	0.449	0.442	0.437	0.434	0.469	0.454	0.529	0.522	0.458	0.450	0.461	0.457	0.440	0.460
ETTh2	96 192 336 720	0.362 0.404	$\frac{0.392}{0.424}$	$0.368 \\ 0.411$	0.389 0.422	0.380 0.428	0.349 0.400 0.432 0.445	$\frac{0.367}{0.412}$	0.389 <u>0.424</u>	0.402 0.435	$0.414 \\ 0.443$	0.373 0.410	$0.394 \\ 0.426$	0.390 0.426	$0.406 \\ 0.444$	$0.388 \\ 0.426$	$0.400 \\ 0.433$	0.877 1.043	0.656 0.731	$0.402 \\ 0.452$	$0.414 \\ 0.452$	0.482 0.591	$0.479 \\ 0.541$	0.429 0.496	0.439 0.487
	Avg.	0.364	0.397	<u>0.372</u>	0.397	0.383	0.407	0.373	0.399	0.396	0.417	0.385	0.408	0.373	0.400	0.387	0.407	0.942	0.684	0.414	0.427	0.563	0.519	0.437	0.449
Weather	192 336	0.202 0.260	0.246	$0.218 \\ 0.274$	0.252 0.294	0.221 0.278	0.296	0.207 0.262	0.250 0.291	$0.212 \\ 0.272$	$0.254 \\ 0.299$	0.217 0.282	$0.253 \\ 0.300$	0.211 0.267	$0.266 \\ 0.310$	0.225	$0.259 \\ 0.297$	$\frac{0.206}{0.272}$	0.277 0.335	$0.219 \\ 0.280$	$0.261 \\ 0.306$	0.237 0.282	$0.295 \\ 0.331$	0.276 0.339	0.336 0.380
	Avg.	0.239	0.269	0.251	0.273	0.258	0.279	0.242	0.272	0.249	0.278	0.255	0.278	0.247	0.289	0.259	0.281	0.259	0.315	0.259	0.287	0.265	0.315	0.309	0.360
Electricity	336	0.154 0.162	0.230 0.248 0.261 0.284	$0.163 \\ 0,175$	0.248 0.262	0.162 0.178	0.253	0.159 0.173	$\frac{0.252}{0.268}$	0.184 0.195	$0.292 \\ 0.302$	$\frac{0.158}{0.178}$	0.248 0.269	0.195 0.206	$0.288 \\ 0.300$	0.215	$0.289 \\ 0.305$	$0.231 \\ 0.246$	0.322 0.337	$0.184 \\ 0.198$	$0.289 \\ 0.300$	0.210 0.223	$0.305 \\ 0.319$	0.201 0.214	0.315 0.329
	Avg.	0.158	0.256	0.172	0.258	0.178	0.270	0.169	0.263	0.194	0.300	0.174	0.264	0.201	0.300	0.216	0.304	0.244	0.334	0.193	0.295	0.225	0.319	0.214	0.327
Traffic	192 336	0.395 0.414	$\frac{0.262}{0.271}$	$0.431 \\ 0.456$	0.262 0.269	0.417 0.433	0.268 0.276 0.283 0.302	0.458 0.486	0.289 0.297	$0.613 \\ 0.642$	$0.359 \\ 0.376$	0.398 0.415	0.261 0.269	0.577 0.588	$0.321 \\ 0.324$	0.540 0.551	$0.354 \\ 0.358$	0.530 0.558	0.293 0.305	0.617 0.629	$0.336 \\ 0.336$	0.598 0.605	$0.370 \\ 0.373$	0.604 0.621	0.373 0.383
	Avg.	0.407	0.268	0.451	0.269	0.428	0.282	0.467	0.294	0.641	0.370	0.409	0.267	0.583	0.323	0.555	0.362	0.550	0.304	0.620	0.336	0.625	0.383	0.610	0.376
Solar-Energy	336	0.226 0.235	0.249 0.261	$\begin{array}{c} \underline{0.228} \\ 0.262 \end{array}$	0.233 0.244	0.233 0.248	0.237 0.261 0.273 0.275	0.231 0.241	0.263 0.268	$0.258 \\ 0.293$	$0.281 \\ 0.311$	$\frac{0.229}{0.243}$	$0.253 \\ 0.269$	0.316 0.347	$0.374 \\ 0.393$	$0.267 \\ 0.290$	$0.310 \\ 0.315$	$0.734 \\ 0.750$	0.725 0.735	$0.296 \\ 0.319$	$0.318 \\ 0.330$	0.320 0.353	$0.398 \\ 0.415$	0.285 0.282	0.380 0.376
S	Avg.	0.223	0.250	0.237	0.233	0.233	0.262	0.230	0.264	0.262	0.288	0.229	0.256	0.324	0.377	0.270	0.307	0.641	0.639	0.301	0.319	0.330	0.401	0.292	0.381

Table 8. Full results of long-term forecasting. The input sequence length L is set to 96 for all baselines. All results are averaged across four different forecasting horizon: $T \in \{96, 192, 336, 720\}$. The best and second-best results are highlighted in **bold** and <u>underlined</u>, respectively.

Me	odels		Filter urs)	DU (202			CM 024)		OF (24)		nTCN 24)	iTrans	former 24b)		ATS (24)	Patch (20	nTST (23)		former		esNet 23)		near 23)
M	etric	MSE	MAE	MSE	MAE	MSE	MAE	MSE	MAE	MSE	MAE	MSE	MAE	MSE	MAE	MSE	MAE	MSE	MAE	MSE	MAE	MSE	MAE
Weather	192 336	0.141 0.184 0.234 0.305	$\frac{0.234}{0.276}$	$\frac{0.188}{0.234}$	0.231 0.268	0.191 0.245	$0.238 \\ 0.285$	0.192 0.244	$0.239 \\ 0.279$	0.196 0.238	$0.245 \\ 0.277$	0.200 0.252	$0.248 \\ 0.287$	0.208 0.264	$0.250 \\ 0.290$	0.194 0.245	$0.241 \\ 0.282$	0.198 0.258	$0.260 \\ 0.314$	0.219 0.278	$0.262 \\ 0.302$	0.216 0.258	0.273 0.307
	Avg.	0.216	0.258	0.218	0.252	0.225	0.263	0.225	0.261	0.224	0.264	0.232	0.270	0.244	0.272	0.226	0.264	0.234	0.292	0.255	0.282	0.242	0.293
Electricity	192 336	0.126 0.143 0.153 0.177	0.237 0.252	0.146 0.163	0.236 <u>0.254</u>	0.153 0.168	$0.248 \\ 0.262$	$\frac{0.145}{0.159}$	$\frac{0.237}{0.255}$	0.143 0.161	$0.239 \\ 0.259$	0.154 0.169	0.250 0.265	0.163 0.180	$0.250 \\ 0.268$	0.147 0.163	$0.240 \\ 0.259$	0.160 0.182	$0.262 \\ 0.282$	0.184 0.198	$0.289 \\ 0.300$	0.152 0.169	0.249 0.267
	Avg.	0.150	0.246	0.158	0.248	0.167	0.261	0.156	0.250	0.156	0.253	0.163	0.258	0.178	0.264	0.159	0.253	0.181	0.279	0.192	0.295	0.166	0.264
Traffic	192 336	0.332 0.348 0.365 0.396	0.246 <u>0.256</u>	0.384 0.395	$0.250 \\ 0.260$	0.379 0.389	0.254 0.255	$\frac{0.363}{0.376}$	$\frac{0.247}{0.258}$	0.379 0.397	$0.261 \\ 0.270$	0.384 0.396	0.273 0.277	0.436 0.453	0.275 0.284	0.379 0.392	$0.256 \\ 0.264$	0.501 0.507	$0.273 \\ 0.279$	0.617 0.629	$0.336 \\ 0.336$	$0.423 \\ 0.436$	0.287 0.296
	Avg.	0.360	0.254	0.394	0.257	0.389	0.259	0.377	0.256	0.396	0.270	0.397	0.281	0.449	0.283	0.391	0.264	0.523	0.284	0.620	0.336	0.434	0.295
Climate	192 336 720		0.489 0.489 0.490	1.098 1.120 1.103	0.511 0.515 0.498	1.118 1.130 1.143	0.510 0.513 0.515	1.362 1.396 1.386	0.570 0.568 0.552	1.125 1.153 1.243	0.523 0.530 0.599	1.055 1.069 1.073	0.496 0.495 0.497	1.073 1.072 1.078	$0.507 \\ \underline{0.495} \\ 0.498$	1.388 1.410 1.395	0.572 0.581 0.575	1.115 1.246 1.236	0.532 0.575 0.584	1.274 1.285 1.347	0.541 0.584 0.626	1.122 1.146 1.158	0.536 0.545 0.545
_	Avg.	1.047	0.490	1.103	0.509	1.123	0.512	1.315	0.555	1.155	0.542	1.060	0.496	1.095	0.509	1.387	0.562	1.170	0.550	1.295	0.569	1.134	0.541

Table 9. Full results of long-term forecasting. The input length L is searched from $\{192, 336, 512, 720\}$ for optimal horizon in the scaling law of TSF (Shi et al., 2024). All results are averaged across four different forecasting horizon: $T \in \{96, 192, 336, 720\}$. The best and second-best results are highlighted in **bold** and <u>underlined</u>, respectively.

M	odels		Filter ırs)	DU (20)	JET 24b)		former 24b)	Led		SOI (20)	FTS 24a)		nTST (23)		former		esNet	Til (20	DE 23)	DLi (20			Net		former
M	etric	MSE	MAE	MSE	MAE	MSE	MAE	MSE	MAE	MSE	MAE	MSE	MAE	MSE	MAE	MSE	MAE	MSE	MAE	MSE	MAE	MSE	MAE	MSE	MAE
PEMS03	12 24 48	0.079	0.185	0.081	0.186	0.093	0.174 0.201 0.236	0.094	0.202	0.083	0.188	0.142	0.259	0.121	0.240	0.118	0.223	0.257	0.371	0.201	0.317	0.085	0.198	0.149	0.275
H	Avg.	0.084	0.191	0.086	<u>0.192</u>	0.096	0.204	0.101	0.210	0.087	<u>0.192</u>	0.151	0.265	0.138	0.253	0.119	0.271	0.271	0.380	0.219	0.295	0.093	0.203	0.167	0.291
MS04	12 24 48	0.080	0.183	0.096	0.203	0.095	0.183 0.205 0.233	0.097	0.209	0.088	0.194	0.153	0.257	0.131	0.256	0.103	0.215	0.292	0.398	0.224	0.340	0.084	0.193	0.177	0.293
PE	Avg.	0.083	0.186	0.096	0.203	0.098	0.207	0.102	0.213	0.091	0.196	0.162	0.273	0.145	0.267	0.109	0.220	0.307	0.405	0.236	0.350	0.085	0.194	0.195	0.308
MS07	12 24 48	0.068	0.166	0.073	0.172	0.088	0.165 0.190 0.215	0.079	0.185	0.073	0.173	0.150	0.262	0.139	0.247	0.101	0.204	0.271	0.383	0.210	0.329	0.119	0.225	0.125	0.244
PE	Avg.	0.071	0.170	0.076	0.176	0.088	0.190	0.087	0.192	0.075	0.173	0.166	0.270	0.181	0.272	0.106	0.208	0.297	0.394	0.241	0.343	0.112	0.211	0.133	0.282
PEMS08		0.079 0.105	0.182 0.214	0.093 <u>0.123</u>	0.191 0.217	0.115 0.186	0.182 0.219 0.235 0.212	0.091 0.145	0.200 0.261	0.104 0.164	0.201 0.253	0.224 0.321	0.281 0.354	0.215 0.315	0.260 0.335	0.141 0.198	0.238 0.283	0.318 0.497	0.409 0.510	0.248 0.440	0.353 0.470	0.122 0.189	0.221 0.270	0.210 0.320	0.310 0.394

Table 10. Full results of short-term forecasting. The input sequence length is set to 96 for all baselines. All results are averaged across four different forecasting horizon: $T \in \{12, 24, 48\}$. The best and second-best results are highlighted in **bold** and <u>underlined</u>, respectively.

Cata	agories							Filter I	Replace								M	οE	
C	ases	Time	Filter	Top	o- <i>K</i>	Rando	om-K	Region	Тор-К	Regio	nThre	C-F	ilter	w/o]	Filter	Static l	Routing	w/o \mathcal{L}_{i}	imp & dyn
M	etric	MSE	MAE	MSE	MAE	MSE	MAE	MSE	MAE	MSE	MAE	MSE	MAE	MSE	MAE	MSE	MAE	MSE	MAE
.	96	0.153	0.199	0.158	0.203	0.158	0.204	0.156	0.202	0.156	0.202	0.155	0.202	0.159	0.204	0.156	0.203	0.156	0.203
ther	192	0.202	0.246	0.207	0.250	0.207	0.251	0.205	0.249	0.202	0.247	0.206	0.249	0.208	0.251	0.205	0.248	0.206	0.248
Weather	336	0.260	0.289	0.264	0.292	0.263	0.292 0.341	0.262 0.342	0.292	0.262	0.291	0.263	0.291	0.265	0.292	0.263	0.290	0.264	0.291
<i>></i>	720	0.342	0.341	0.344	0.343	0.342			0.342	0.341	0.341	0.343	0.342	0.345	0.345	0.343	0.342	0.344	0.344
!	Avg.	0.239	0.269	0.243	0.272	0.243	0.272	0.241	0.271	0.241	0.270	0.242	0.271	0.244	0.273	0.242	0.271	0.243	0.272
Ľ.	96	0.133	0.230	0.138	0.235	0.137	0.235	0.139	0.235	0.138	0.234	0.137	0.234	0.139	0.237	0.137	0.234	0.136	0.233
ici	192	0.154	0.248	0.163	0.255	0.161	0.254	0.163	0.255	0.164	0.257	0.159	0.252	0.159	0.252	0.156	0.250	0.155	0.250
Electricity	336	0.162	0.261 0.284	0.168	0.266	0.174	0.270 0.297	0.169 0.199	0.265 0.295	0.166	0.264 0.314	0.169	0.267 0.308	0.168	0.265	0.167 0.195	0.264 0.290	0.166	0.263
回	720	0.184		0.200	0.297	0.200		0.199		0.220		0.214		0.200	0.298	0.193		0.193	0.288
	Avg.	0.158	0.256	0.167	0.263	0.168	0.264	0.168	0.263	0.172	0.267	0.170	0.265	0.167	0.263	0.164	0.260	0.163	0.259
	96	0.375	0.251	0.379	0.253	0.378	0.253	0.377	0.251	0.378	0.251	0.379	0.252	0.379	0.254	0.377	0.253	0.378	0.254
- ju	192	0.395	0.262	0.404	0.265	0.402	0.264	0.403	0.263	0.406	0.264	0.405	0.264	0.404	0.266	0.398	0.264	0.397	0.264
Traffic	336	0.414	0.271	0.420	0.274	0.418	0.273	0.416	0.272	0.417	0.275	0.418	0.274	0.422	0.275	0.417	0.273	0.417	0.272
	720	0.445	0.289	0.449	0.293	0.448	0.292	0.449	0.292	0.447	0.291	0.448	0.291	0.450	0.295	0.447	0.292	0.448	0.293
	Avg.	0.407	0.268	0.413	0.271	0.412	0.271	0.411	<u>0.270</u>	0.412	0.271	0.413	0.271	0.414	0.273	<u>0.410</u>	0.271	0.410	0.271
53	96	0.193	0.223	0.203	0.229	0.198	0.225	0.202	0.224	0.204	0.225	0.203	0.225	0.201	0.234	0.196	0.224	0.194	0.224
ner	192	0.226	0.249	0.225	0.255	0.228	0.257	0.225	0.254	0.224	0.254	0.233	0.257	0.230	0.262	0.230	0.262	0.227	0.262
뛴	336	0.235	0.261	0.249	0.270	0.244	0.269	0.253	0.271	0.254	0.274	0.251	0.273	0.249	0.272	0.242	0.269	0.242	0.270
Solar-Energy	720	0.239	0.268	0.248	0.276	0.252	0.280	0.250	0.277	0.256	0.281	0.250	0.278	0.256	0.280	0.245	0.276	0.244	0.275
	Avg.	0.223	0.250	0.231	0.258	0.231	0.258	0.233	0.257	0.235	0.259	0.234	0.258	0.234	0.262	0.228	0.258	0.227	0.258
	96	0.370	0.394	0.379	0.399	0.377	0.396	0.379	0.398	0.379	0.398	0.377	0.399	0.379	0.398	0.374	0.397	0.374	0.394
딥	192	0.413	0.420	0.432	0.429	0.430	0.427	0.432	0.429	0.434	0.428	0.424	0.428	0.431	0.429	0.421	0.424	0.421	0.423
ETTh1	336	0.450	0.440	0.478	0.454	0.475	0.453	0.479	0.454	0.469	0.449	0.467	0.452	0.475	0.453	0.460	0.446	0.460	0.445
ш	720	0.448	0.457	0.474	0.468	0.482	0.473	0.475	0.469	0.466	0.467	0.457	0.463	0.481	0.471	0.465	0.467	0.465	0.467
	Avg.	0.420	0.428	0.441	0.438	0.441	0.437	0.441	0.438	0.437	0.436	<u>0.431</u>	0.436	0.442	0.438	0.440	0.434	0.430	<u>0.432</u>
	96	0.169	0.255	0.172	0.257	0.172	0.257	0.170	0.257	0.172	0.257	0.172	0.258	0.173	0.257	0.172	0.256	0.171	0.256
n2	192	0.235	0.299	0.237	0.300	0.238	0.301	0.233	0.299	0.237	0.299	0.235	0.300	0.237	0.300	0.236	0.298	0.235	0.298
ETTm2	336	0.293	0.336	0.298	0.340	0.296	0.338	0.298	0.340	0.297	0.340	0.299	0.342	0.298	0.340	0.295	0.337	0.294	0.336
山	720	0.390	0.393	0.395	0.398	0.396	0.397	0.392	0.396	0.399	0.398	0.400	0.400	0.400	0.399	0.392	0.396	0.393	0.397
	Avg.	0.272	0.321	0.276	0.324	0.276	0.323	0.273	0.323	0.276	0.324	0.277	0.325	0.277	0.324	0.274	0.322	0.273	0.322
	12	0.064	0.162	0.065	0.165	0.066	0.165	0.064	0.164	0.065	0.163	0.064	0.164	0.065	0.164	0.064	0.163	0.064	0.162
808	24	0.079	0.182	0.081	0.185	0.081	0.184	0.081	0.186	0.081	0.185	0.082	0.185	0.082	0.186	0.080	0.184	0.080	0.183
PEMS08	48	0.105	0.214	0.112	0.224	0.108	0.217	0.110	0.219	0.108	0.219	0.111	0.222	0.110	0.223	0.108	0.216	0.108	0.217
E	Avg.	0.083	0.186	0.086	0.191	0.085	0.189	0.085	0.190	0.085	0.189	0.086	0.190	0.086	0.191	0.084	0.188	0.084	0.187

Table 11. Component ablation of TimeFilter.

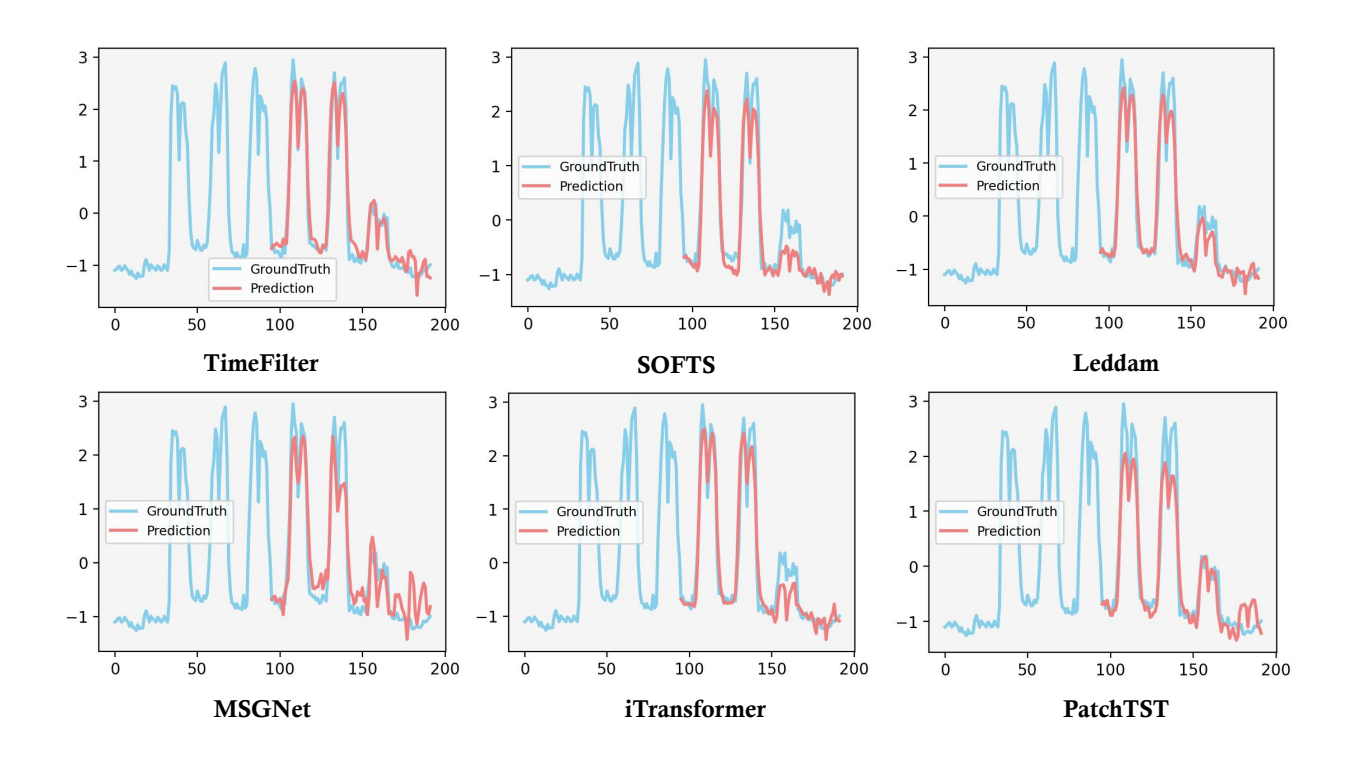


Figure 7. Visualization of predictions from different models on the Electricity dataset.

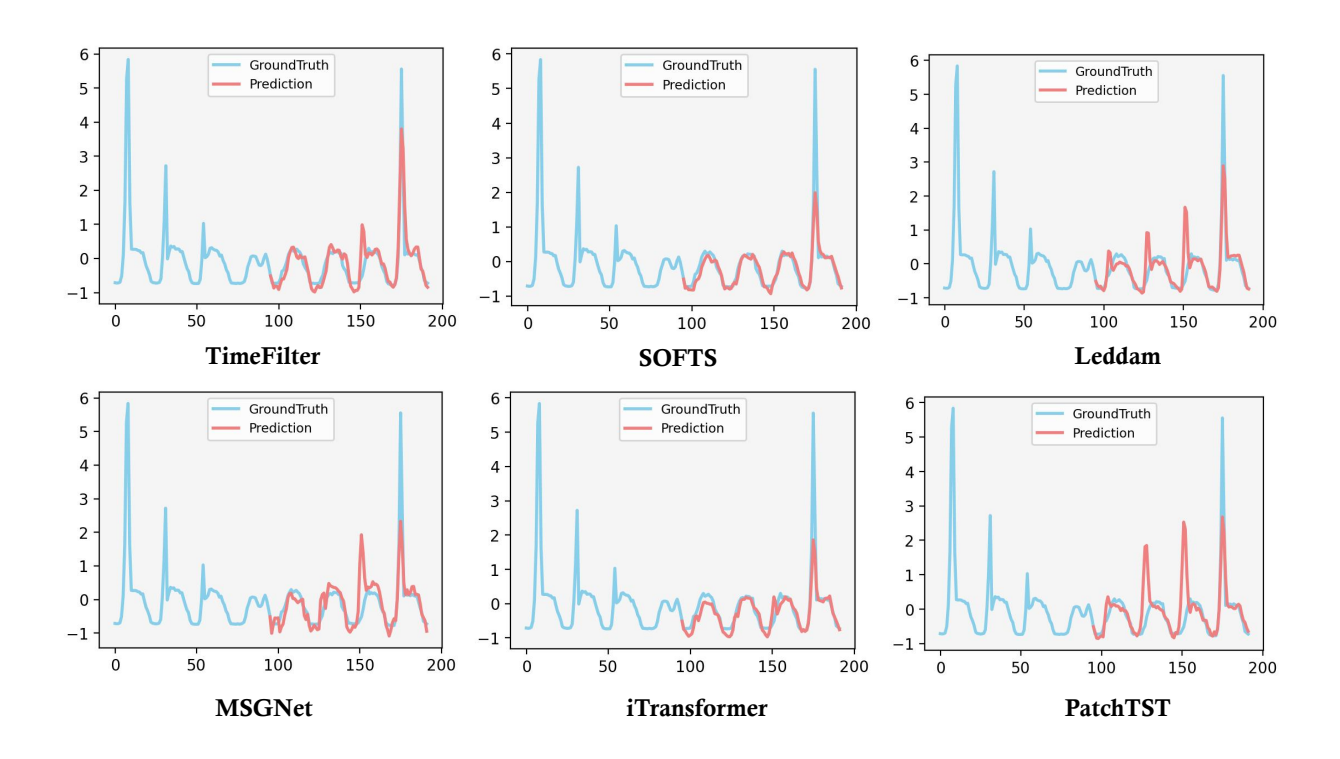


Figure 8. Visualization of predictions from different models on the Traffic dataset.

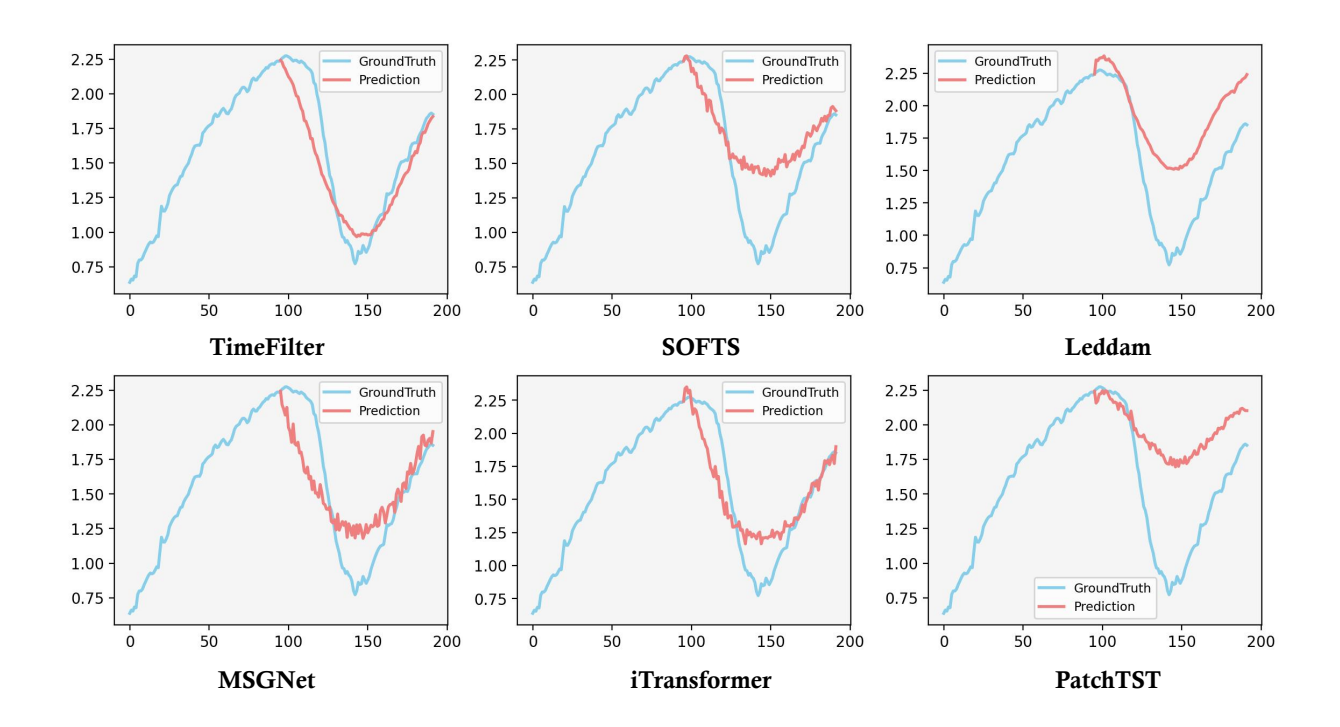


Figure 9. Visualization of predictions from different models on the Weather dataset.

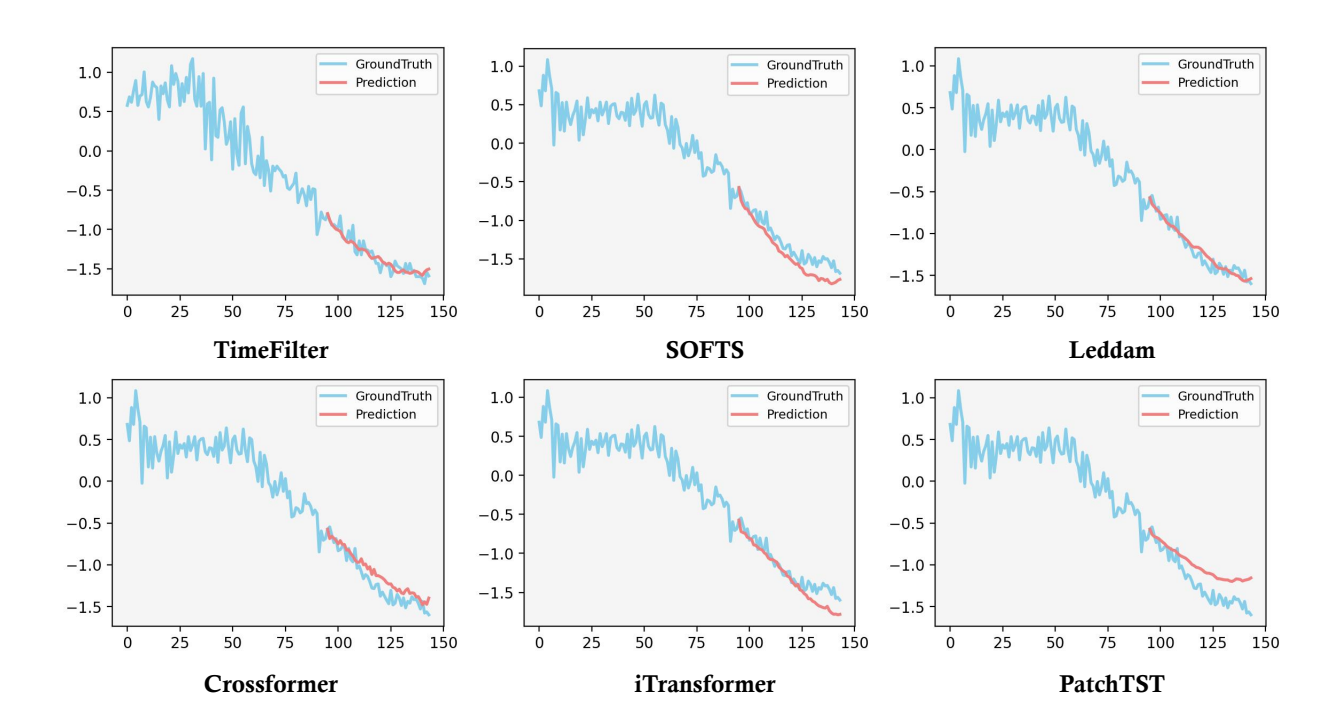


Figure 10. Visualization of predictions from different models on the PEMS08 dataset.